INSTITUTE FOR DEFENSE ANALYSES

Rapid and Automatic Reachability Estimation of Electric Propulsion Spacecraft

Prashant R. Patel, Project Leader
Daniel J. Scheeres

September 2023

IDA Document NS D-3336

Log: H 23-000008

INSTITUTE FOR DEFENSE ANALYSES
730 East Glebe Road
Alexandria, Virginia 22305

About This Publication

This work was conducted by the IDA Systems and Analyses Center, Central Research Program, project C7265, "Space Conference Outreach." The views, opinions, and findings should not be construed as representing the official position of either the Department of Defense or the sponsoring organization.

For More Information

Prashant R. Patel, Project Leader
prashant.patel@ida.org, (703) 575-1439

David E. Hunter, Director, Cost Analysis and Research Division
dhunter@ida.org, (703) 575-4686

Copyright Notice

INSTITUTE FOR DEFENSE ANALYSES

IDA Document NS D-33362

Rapid and Automatic Reachability Estimation of Electric Propulsion Spacecraft

Prashant R. Patel
Daniel J. Scheeres

Rapid and Automatic Reachability Estimation of Electric Propulsion Spacecraft

Prashant R. Patel[1*] and Daniel J. Scheeres[2]

[1*]Cost Analysis and Research Division, Institute for Defense Analyses, 730 East Glebe Road, Alexandria, 22305, VA, USA.

[2]Ann and H.J. Smead Aerospace Engineering Sciences, University of Colorado, 3775 Discovery Drive, Boulder, 80303, CO, USA.

*Corresponding author(s). E-mail(s): prashant.r.patel@gmail.com;
Contributing authors: scheeres@colorado.edu;

Abstract

Reachable and controllable sets for electric propulsion spacecraft are important to many problems including: dynamic replanning, robust mission design, space situational awareness, assessing advanced concepts, and threat assessments. Current methods result in a two-point boundary value problem or are limited in their application. The reachable and controllable problem is solved using an multistage indirect approach. The paper demonstrates our formulation enables rapid, reliable, and autonomous estimates of the reachable and controllable sets. Numerical examples show that the algorithms work in strong multibody environments (i.e., flybys) and incorporates uncertainty in initial conditions. These conditions make the algorithm suitable for space situational awareness and cislunar applications.

Keywords: Reachability, electric propulsion, automated, space situational awareness

1 Introduction

Range as a function of fuel is an important concept, and it exerts a key influence on the design of vehicles and operations. It is needed for dynamic fleet

replanning, context-based mission orders, robust mission design, situational awareness, autonomous operations, and developing advanced concepts such as refueling tradeoffs.

Air, land, and sea domains have long used fuel-range calculations for design and operations. These domains benefit from range being independent of position, with the benefit that a vehicle's location changes, the range remains known and does not change. This position-independent range concept greatly simplifies design and operations. Designers benefit because a single design can satisfy a global range requirement. Operational planners benefit because assets can be repositioned, and their range does not change.

In contrast, space dynamics result in position-dependent range, meaning that the range of a space vehicle varies with its current location. In addition, the range cannot be expressed as a single value. Instead, range must be described as the potential envelope of orbits a spacecraft can achieve (the reachable set). Positional reachability is a two-dimensional space. Orbital reachability (position and velocity) is a five-dimensional space. These unique properties of the space domain require continually recomputing reachability as the spacecraft moves.

The position-dependent nature of spacecraft reachability creates a further complication, as the location of a spacecraft may not be exactly known. Instead, sensors may only provide an estimate of the spacecraft's position and/or velocity. Space situational awareness (SSA) applications would benefit greatly from being able to quickly and accurately estimate the reachable set while accounting for uncertainty in the initial conditions.

This paper describes our approach to rapidly and automatically estimating the reachability of electric propulsion (EP) spacecraft. The algorithm has proven to be fast and stable, works in multibody (e.g., cislunar) dynamics, requires no user-defined initial guess, and can account for uncertainty in sensor measurements using the approach Holzinger defined[1]. The algorithm is further extended to account for initial ΔV maneuvers.

1.1 Literature Review

Reachability of space vehicles is a widely studied topic[1–5], relating to a variety of applications including SSA, mission planning, trajectory optimization, and safety. Accordingly, researchers have devised numerous ways to formulate and solve the reachability problem. Reachability problems are commonly formulated as an optimal control problems where the distance reached is maximized[1, 4, 5]. This section highlights several approaches to solving optimal control problems[6] and contrasts them with this paper's approach.

Spacecraft maneuver is analyzed based on the propulsion system, as that drives the dynamical approximations that can be used. Chemical propulsion is commonly approximated as an instantaneous change in the velocity of the spacecraft. The impulsive change in velocity is commonly referred to as a ΔV maneuver. The ΔV approximation is accurate when the thruster provides a

relatively high thrust-to-weight ratio over short burn times. This approximation decouples the trajectory and the thruster, as the thruster characteristics do not appear in the dynamical equations.

Optimal impulsive transfers have some well known classic solutions, such as the Hohmann transfer. Holzinger[2] demonstrated that time-independent reachable sets for chemical propulsion can be readily computed. Their formulation elegantly provides insights for mission planning and recovers classical solutions to optimal ΔV orbit transfers.

Compared to chemical propulsion, electric propulsion provides lower thrust-to-weight ratios, longer thrust times, and better propellant utilization. Electric propulsion can be modeled several ways–one being to model it as a many small ΔV maneuvers[7], where the magnitude of the maneuver is restricted by the segment duration and thruster characteristics. Another approach is to embed the thruster characteristics within the equations of motion and fully integrate them. Both approaches require many more controls than the impulsive formulation and couples the dynamics and thruster characteristics.

Indirect continuous formulations are commonly used to solve optimal electric propulsion trajectories, including reachability problems. Holzinger[1] derived the general reachability equations for the continuous indirect formulation and presented various dynamical problems. The downside of indirect continuous formulations are that they result in a two-point boundary value problem, which can be difficult to solve[8].

Many approaches have been developed to solve two-point boundary value problems[6], but they require a user-supplied initial guess. One alternative, to a user supplied initial guess, is to use insights to find close approximations to the problem of interest. Thorne[9] derived a set of formulas that produce approximate values for both the initial Lagrange co-states and the associated optimal flight time needed to solve the minimum-time, continuous-thrust orbital trajectory design problem. Thorne's formulas are especially accurate for either high-thrust or short-duration transfers starting from circular conditions, but they have also been used effectively to solve low-thrust, non-circular, three-dimensional problems with the continuation method. Currently, a method for approximating the initial co-states of the reachability problem does not exist. Another approach to avoiding the user supplied initial guess issue is to leverage leverage stochastic approaches[4, 5]. These auto generate a population of solutions that are iteratively improved.

Generating functions offer a distinctly different approach as they capture the full solution flow[10]. Bando[11] uses a power series expansion of the generating function to identify low-thrust transfers in the Hill frame.

The contribution of this work to the literature is twofold. First, a rapid and automatic algorithm for estimating the reachability of electric-propulsion spacecraft is developed. The elimination of the two-point boundary-value problem obviates the need for an initial guess, thereby increasing the algorithm's predictability and stability. Second, the use of an indirect multistage formulation is novel and has not been previously used for this problem.

1.2 Paper layout

The paper begins by discussing the indirect multistage formulation and the derivation of the reachable set equations. The Formulation and Derivation section provides the general and specific equations used in implementing the algorithm, including the Gaussian level set and ΔV boundary conditions. In the Reachable Set Algorithm section, two different approaches to estimating the reachable set are presented. The Fast First Order Estimate provides a fast approach to estimating the reachable set, whereas the Open-Loop Exact Algorithm provides an iterative approach to obtain a more exact estimate. The limitations and tradeoffs of the two different algorithms are then discussed. The Numerical Examples section implements the algorithms and demonstrates the algorithms in two-body problems, multibody dynamics, and controllability/reachability problems. The cases used in the Numerical Examples section include the Gaussian level set boundary conditions, thereby showing that the algorithm can be used for some SSA applications. Lastly, the Conclusion section provides a discussion of this work's value and applications.

2 Formulation and Derivation

The formulation and derivation section begins by reviewing the indirect multistage formulation and deriving the co-state equations and optimal conditions. Next, the equations of motion, cost function, constraints for the electric propulsion reachability problem are discussed. Finally, the control law and co-state dynamics are derived.

2.1 Indirect Multistage Formulation

The indirect multistage formulation is the indirect analog to direct formulations. Each stage takes the current state and the control (for that stage) as inputs and provides the updated state as outputs. This process requires that states be consistent across the trajectory, although the controls can vary. The dynamics can change at each stage as well so long as the states are consistent.

The paper uses a controlled dynamical system defined by:

$$\dot{\boldsymbol{x}} = \boldsymbol{f}(\boldsymbol{x}, t, \boldsymbol{u}, \boldsymbol{p}) \tag{1}$$

Bold indicates a vector or matrix, whereas a normal font indicates a scalar quantity. $\boldsymbol{x}$ represents the state vector; $\boldsymbol{u}$ is the control vector, which is in general a function of time; t is time; and $\boldsymbol{p}$ is a set of parameters that are constant in the system.

This system can be transformed into a set of indirect multi-stage formulation equations[8]. A trajectory segment i is governed by:

$$\boldsymbol{x}^{i+1} = \boldsymbol{F}^i(\boldsymbol{x}^i, t^i, \boldsymbol{u}^i, \boldsymbol{p}) \tag{2}$$

where

$$\boldsymbol{F}^i = \boldsymbol{x}^i + \int_{t_i}^{t_{i+1}} \dot{\boldsymbol{x}} dt = \boldsymbol{x}^i + \int_{t_i}^{t_{i+1}} \boldsymbol{f}(\boldsymbol{x}, t, \boldsymbol{u}, \boldsymbol{p}) dt \tag{3}$$

A trajectory is then composed of a series of N trajectory segments, where $N \geq 1$. For a multi-segment trajectory, Eq. (2) can be integrated from i to $i+1$, then recursively use $i+1$ to obtain $i+2$, and so on. The controls $\boldsymbol{u}(i)$ are fixed on each segment. This is not a significant limitation, as time varying inputs can be modeled by having $\boldsymbol{u}(i)$ represent the constant coefficients of a time varying function.

The cost function for a multi-stage formulation is given by:

$$J = \phi(\boldsymbol{x}^N, N) + \sum_i L(i, \boldsymbol{x}^i, \boldsymbol{u}^i) \tag{4}$$

where $\phi(\boldsymbol{x}_N, N)$ is the terminal cost function and $L(i, \boldsymbol{x}, \boldsymbol{u}) = L^i$ is the integral cost function evaluated at the ith step. The Hamiltonian is then defined as:

$$H = \sum_i H^i \tag{5}$$

$$H^i = \boldsymbol{\lambda}^{i+1} \cdot \boldsymbol{F}^i + L^i + \sum_k \nu_k C_k \tag{6}$$

For notational convenience later, the adjoints are specified with an index $i+1$, and C represents the per-stage constraints.

Taking the partial with respect to $\boldsymbol{x}$ yields the dynamics equations for the co-states

$$H^i_{\boldsymbol{x}} = \boldsymbol{\lambda}^i = \boldsymbol{F}^{iT}_{\boldsymbol{x}} \boldsymbol{\lambda}^{i+1} + L^i_{\boldsymbol{x}} + \sum_k \nu_k C_{k,\boldsymbol{x}} \tag{7}$$

where T is the transpose operator. The control law is then given by Pontryagin's principle, by taking the partial of the Hamiltonian with respect to the control and solving for when this quantity is zero (hence, an extremal), as shown:

$$H^i_{\boldsymbol{u}} = \boldsymbol{0} = \boldsymbol{F}^{iT}_{\boldsymbol{u}} \boldsymbol{\lambda}^{i+1} + L^i_{\boldsymbol{u}} + \sum_k \nu^k C^k_{\boldsymbol{u}} \tag{8}$$

The initial and terminal conditions are given as:

$$\boldsymbol{C}^0(\boldsymbol{x}) = 0 \quad \boldsymbol{C}^N(\boldsymbol{x}) = 0 \tag{9}$$

resulting in the initial and terminal co-states being:

$$\boldsymbol{\lambda}^0 = \nu^0 \cdot \boldsymbol{C}^0_{\boldsymbol{x}} \quad \boldsymbol{\lambda}^N = \phi_{\boldsymbol{x}} + \nu^N \cdot \boldsymbol{C}^N_{\boldsymbol{x}} \tag{10}$$

Taken together, these formulas represent the general equations for the multi-stage optimization problem.

2.2 Reachable Set Equations

This section covers the specific equations that will be used in the algorithms. The first step is to define the state dynamics, cost function, constraints, control law, and boundary conditions. The equations of motion used in this paper are stated in an inertial frame with an arbitrary origin:

$$\dot{\boldsymbol{x}} = \begin{bmatrix} \dot{\boldsymbol{r}} \\ \dot{\boldsymbol{v}} \\ \dot{n} \end{bmatrix} = \begin{bmatrix} \boldsymbol{v} \\ \sum_j -\frac{\mu^j}{\|\boldsymbol{r}-\boldsymbol{r}^j\|^3}(\boldsymbol{r}-\boldsymbol{r}^j) + n\boldsymbol{T} \\ n^2 \frac{T_{mag}}{c} \end{bmatrix} \tag{11}$$

where μ_j is the gravitational parameter of the attracting body located at $\boldsymbol{r}_j$, $\boldsymbol{T}$ is the thrust vector, T_{mag} is the magnitude of thrust, $\boldsymbol{r}$ is the position vector, $\boldsymbol{v}$ is the velocity, n is the inverse mass, and c is one Earth gravity times the specific impulse. The cost function is defined as:

$$J = -\min \quad \hat{\boldsymbol{z}} \cdot \boldsymbol{x}^N \tag{12}$$

The cost function represents maximizing $\boldsymbol{x}^N$ along the direction $\hat{\boldsymbol{z}}$, which is a specified unit vector that will be swept over to sample the reachable set. For consistency between the dynamics and engine $\|\boldsymbol{T}\| = T_{mag}$ and $0 \leq \|\boldsymbol{T}\| \leq T_{max}$. These conditions require the supplied thrust must be less than the maximum allowable thrust, T_{max}, and that the total thrust and T_{mag} be equal. The latter constraint simply enforces that the thrust used to generate acceleration is equal to the thrust supplied by the engine.

The Hamiltonian is then:

$$H^i = \boldsymbol{F}^{iT}\boldsymbol{\lambda}^{i+1} + \nu_1(\|\boldsymbol{T}\| - T_{mag}) + \nu_2(\frac{1}{2}T_{mag}^2 - \frac{1}{2}T_{max}^2) \tag{13}$$

The co-state equation is:

$$H_{\boldsymbol{x}}^i = \boldsymbol{\lambda}^i = \boldsymbol{F}_{\boldsymbol{x}}^{iT}\boldsymbol{\lambda}^{i+1} \tag{14}$$

and is formulated to move backwards in time. The term $\boldsymbol{F}_{\boldsymbol{x}}^{\boldsymbol{i}}$ is the state transition matrix at the end of the segment. It is given by

$$\boldsymbol{F}_{\boldsymbol{x}}^{\boldsymbol{i}} = \frac{\partial \boldsymbol{x}^{i+1}}{\partial \boldsymbol{x}^i} = \Phi(t^{i+1}, t^i) = \int_{t^i}^{t^{i+1}} \begin{bmatrix} \boldsymbol{0} & \boldsymbol{I} & \boldsymbol{0} \\ \frac{\partial \dot{\boldsymbol{v}}}{\partial \boldsymbol{r}} & \boldsymbol{0} & \boldsymbol{T} \\ 0 & 0 & 2n\frac{T_{mag}}{c} \end{bmatrix} \Phi(t, t^i)dt \tag{15}$$

where Φ is the state transition matrix. The initial conditions for $\Phi(i, i) = \boldsymbol{I}$.

The control law is defined by:

$$H_{\boldsymbol{u}} = 0 = \boldsymbol{F}_{\boldsymbol{u}}^{iT}\boldsymbol{\lambda}^{i+1} + \nu_1 \begin{bmatrix} \frac{\boldsymbol{T}}{\|\boldsymbol{T}\|} \\ -1 \end{bmatrix} + \nu_2 \begin{bmatrix} 0 \\ T_{mag} \end{bmatrix} \tag{16}$$

and

$$\boldsymbol{F_u^i} = \frac{\partial \boldsymbol{x}^{i+1}}{\partial \boldsymbol{u}^i} = \Omega(t^{i+1}, t^i) = \int_{t^i}^{t^{i+1}} \begin{bmatrix} \boldsymbol{0}_{3\times3} & \boldsymbol{I}_{3\times3} & \boldsymbol{0}_{3\times1} \\ \frac{\partial \dot{\boldsymbol{v}}}{\partial \boldsymbol{r}} & \boldsymbol{0}_{3\times3} & \boldsymbol{T} \\ \boldsymbol{0}_{1\times3} & \boldsymbol{0}_{1\times3} & 2n\frac{T_{mag}}{c} \end{bmatrix} \Omega(t, t^i) + \begin{bmatrix} \boldsymbol{0}_{3\times3} & \boldsymbol{0}_{3\times1} \\ n\boldsymbol{I}_{3\times3} & \boldsymbol{0}_{3\times1} \\ \boldsymbol{0}_{1\times3} & \frac{n^2}{c} \end{bmatrix} dt \tag{17}$$

The term Ω is analogous to the impulse response matrix for linear systems. The initial condition for the integral is given by $\Omega(i, i) = 0$. Solving Eq. (16) and satisfying the constraints results in:

$$T_{mag} = T_{max}, \quad and \quad \boldsymbol{T} = -T_{max}\frac{\boldsymbol{F_T^T}\boldsymbol{\lambda}}{\|\boldsymbol{F_T^T}\boldsymbol{\lambda}\|} \tag{18}$$

where

$$\nu_1 = \|\boldsymbol{F_T^T}\boldsymbol{\lambda}^{i+1}\| \tag{19}$$

$$\nu_2 = \frac{\nu_1 - \boldsymbol{F}_{T_{mag}}^T\boldsymbol{\lambda}^{i+1}}{T_{max}} \tag{20}$$

In these equations, $\boldsymbol{F_T}$ is the columns of $\boldsymbol{F_u}$ associated with the thrust direction $\boldsymbol{T}$. Similarly, $\boldsymbol{F}_{T_{mag}}$ is the column of $\boldsymbol{F_u}$ associated with T_{mag}.

Initial state uncertainty can be readily incorporated by using the same formulation as Holzinger[1]:

$$\boldsymbol{C}^0 = \frac{1}{2}\boldsymbol{\delta x}_0^T E \boldsymbol{\delta x}_0 - \frac{1}{2}d^2 \tag{21}$$

$$\boldsymbol{C}_{\boldsymbol{x}}^0 = E\boldsymbol{\delta x}_0 \tag{22}$$

where E is a symmetric full rank matrix and with d defines the ellipsoid set that the initial states lie on. Combining these equations results in

$$\boldsymbol{\delta x}_0 = -d\frac{E^{-1}\boldsymbol{\lambda}_0}{\sqrt{\boldsymbol{\lambda}_0^T E^{-1}\boldsymbol{\lambda}_0}} \tag{23}$$

In Eq. (23), $\boldsymbol{\delta x}_0$ is a function of $\boldsymbol{\lambda}_0$, while Holzinger[1] makes the initial co-states a function of the initial states. This paper's approach differs because the co-states are known and they define the type of reachable set. The states by themselves do not provide the necessary information. This attribute makes it more straightforward to solve for the change in initial states as a function of the co-states. Sweeping over the deviation in the states, imposes a constraint on the terminal co-states which has to be satisfied. For example, if physical reachability is desired, then the terminal co-states associated with velocity and inverse mass must equal $\boldsymbol{0}$.

In cases where there is uncertainty in only some of the states or the uncertainty is decoupled (e.g., position or velocity), Eq. (23) is still valid but would be applied to those sub-elements only. For example, if there is uncertainty in position estimates but not velocity, Eq. (23) would be applied to the positional states.

Additionally, a similar formulation can be used to account for initial ΔV maneuvers.

$$\boldsymbol{C}^1 = \frac{1}{2}\boldsymbol{\Delta V}^T\boldsymbol{\Delta V} - \frac{1}{2}\Delta V_{max}^2 \tag{24}$$

$$\boldsymbol{C}_{\boldsymbol{x}}^1 = \boldsymbol{\Delta V} \tag{25}$$

$$\boldsymbol{\delta v}_0 = \Delta V = -\Delta V_{max}\frac{\boldsymbol{\lambda}_v}{\|\boldsymbol{\lambda}_v\|} \tag{26}$$

Because the magnitude of the ΔV maneuver is equal to ΔV_{max}, a constraint for the mass is unnecessary as it is known.

The indirect multi-stage formulation has several significant differences from the indirect continuous formulation. For example, in the indirect continuous formulation, the control is a function of the current states and co-states, which results in a single-state/co-state transition matrix[1]. A unified-state/co-state transition matrix is not possible for the indirect multi-stage approach, as the control cannot be eliminated. In Eq. (18) the control, $\boldsymbol{T}$, is defined in terms of $\boldsymbol{F_T}$ and $\boldsymbol{\lambda}^{i+1}$. Since $\boldsymbol{F_T}$ is an implicit function of $\boldsymbol{T}$, a unified-state/co-state transition matrix cannot be created. For a more detailed discussion of why these differences exist we refer the reader to Patel[12].

In this subsection, the specific indirect multistage equations used in the algorithms were derived. Sufficient information now exists to estimate the reachable and controllable set even when the states are uncertain. Significantly, T_{max} (see Eq. (18)) does not affect the direction of thrust, allowing us to integrate along the unpowered trajectory and then conduct trade studies by sweeping over various thrust levels.

3 Reachable Set Algorithm

In this section two algorithms are developed that can estimate the reachable set. The first algorithm, called fast first order estimate (FFOE), is designed to provide a fast estimate of the reachable set. The second algorithm is designed to provide a more precise estimate of the reachable set, at the expense of speed. The details of each algorithm will be discussed along with the tradeoffs associated with each algorithm.

3.1 Fast First Order Estimate

The FFOE algorithm is designed to provide a good and fast estimate of the reachable set. First the algorithm will be constructed then a discussion on the why it provides reasonably accurate estimates will be provided.

The FFOE algorithm begins by integrating and obtaining the partials ($\boldsymbol{F_x}$ and $\boldsymbol{F_u}$) along a non thrusting trajectory. These partials will then be used to estimate the control. To estimate the control, we select the values of $\hat{\boldsymbol{z}}$ from a unit ball and use them to initialize the terminal co-states. These co-states are then propagated backwards in stages using Eq. (14), and the control law is

calculated from Eq. (18), where $\boldsymbol{F_x}$ and $\boldsymbol{F_u}$ are obtained from the non thrusting control law. The final step is to integrate Eq. (11) using the derived control law to compute the reachable set. Formally, the algorithm is shown in Alg. (1).

Algorithm 1 FFOE algorithm

$x^0 \leftarrow$ initial conditions
$t^0 \leftarrow$ start time
$dt \leftarrow$ segment duration
$Seg \leftarrow$ number of segments
$\boldsymbol{T} \leftarrow \mathbf{0}$
$i \leftarrow 0$
while $i < Seg$ **do**
  $\boldsymbol{x}^{i+1}, \boldsymbol{F}_{\boldsymbol{x}}^i, \boldsymbol{F}_{\boldsymbol{u}}^i \leftarrow \boldsymbol{F}^i(\boldsymbol{x}^i, \boldsymbol{T}^i, t_0, t_0 + dt)$
  $t_0 \leftarrow t_0 + dt$
  $i \leftarrow i + 1$
end while
$j \leftarrow 0$
$N \leftarrow$ Number of sample points
while $j < N$ **do**
  $i \leftarrow Seg - 1$
  $\boldsymbol{\lambda}^{Seg} \leftarrow$ from unit ball
  while $i \geq 0$ **do**
    $\boldsymbol{T}^{i,j} \leftarrow$ Eq. (18)
    $\boldsymbol{\lambda}^i \leftarrow$ Eq. (14)
    $i \leftarrow i - 1$
  end while
  $j \leftarrow j + 1$
end while
$j \leftarrow 0$
while $j < N$ **do**
  $i \leftarrow 0$
  while $i < Seg$ **do**
    $\boldsymbol{x}^{i+1} \leftarrow \boldsymbol{F}^i(\boldsymbol{x}^i, \boldsymbol{T}^{i,j}, t_0, t_0 + dt)$
    $t_0 \leftarrow t_0 + dt$
    $i \leftarrow i + 1$
  end while
  $j \leftarrow j + 1$
end while

3.2 Open-Loop Exact Algorithm

The open-loop exact (OLE) solution is an open-loop method that iteratively updates the control law to estimate the exact reachable set. The OLE algorithm uses the FFOE algorithm as a starting point, but at each iteration uses

the thrusting partials from the prior run. Thus the OLE algorithm should be more accurate, but at the expense of additional computational time and potential convergence issues.

The OLE algorithm begins by using the FFOE algorithm to estimate the control law. Then for each $\hat{z}$ and associated control law, the OLE algorithm computes the trajectory partials. Next, using the same $\hat{z}$ OLE computes the new control law with the updated trajectory partials. Finally, OLE compare the change in the cost function between the prior and current iteration. If the change in cost function between iterations is less than a specified precision, or if the maximum number of iterations is reached, the algorithm terminates.

3.3 Algorithmic Performance, Limitations, and Trade-offs

The FFOE algorithm generally did a good job of estimating the reachable set (for some examples, see Fig. (2) and Fig. (3)) but tests did identify some limitations. This section, lays out a series of hypothesis for why the FFOE algorithm performed reasonably well and highlight cases where users should validate the results with other methods.

The FFOE's control law is a first-order update to the natural (unpowerd) trajectory, which is an optimal solution. When the partials of the natural trajectory are close to the partials of the powered trajectory then the FFOE algorithm should provide a good estimate. The partials should be close when the thrust is"small". The test cases (see section Numerical Examples) show that the FFOE algorithm performs well in two-body and multi-body cases for low thrust and short timescales. At the moment "short" timescales or "small" thrust is not well defined for this problem. Exploring how time and thrust effect the results is subject of on-going research.

Testing also identified several conditions where the FFOE algorithm failed. When the reachable set encapsulated a gravitational center, the FFOE and OLE algorithms both produced poor solutions. The FFOE algorithm continued to produce a solution, but it was a gross underestimate of the reachable set. On the other hand, the OLE algorithm failed to converge. The FFOE algorithm performed poorly because it did not take full advantage of the gravitational encounter, whereas the OLE algorithm attempted to pass arbitrarily close to the center of the body, leading to non convergence.

Both algorithms also had trouble on some multi revolution cases. Specifically, when the reachable set encapsulated the reference trajectory. This issue can possibly be resolved by using alternative coordinate frames (e.g., polar coordinates), if the particular application allows for non-Cartesian coordinates.

The OLE algorithm had a unique failure mode, which the FFOE did not exhibit. In some cases the OLE algorithm would only map out part of the reachable set but miss large sections of it. This behavior occurred when the reachable set was concave. This behavior of the OLE algorithm occurs because the cost function is a projection operator, which does not guarantee that the solution will be parallel to $\hat{\lambda}$ but rather guarantees only that the projection of the solution onto $\hat{\lambda}$ will be maximized. Fig. (1) provides a visual representation

of when the OLE algorithm can produce incomplete results. The entire concave region maps to the converged point in Fig. (1) or its counterpart on the other side of the projection direction line due to the use of a projection operator as the cost function.

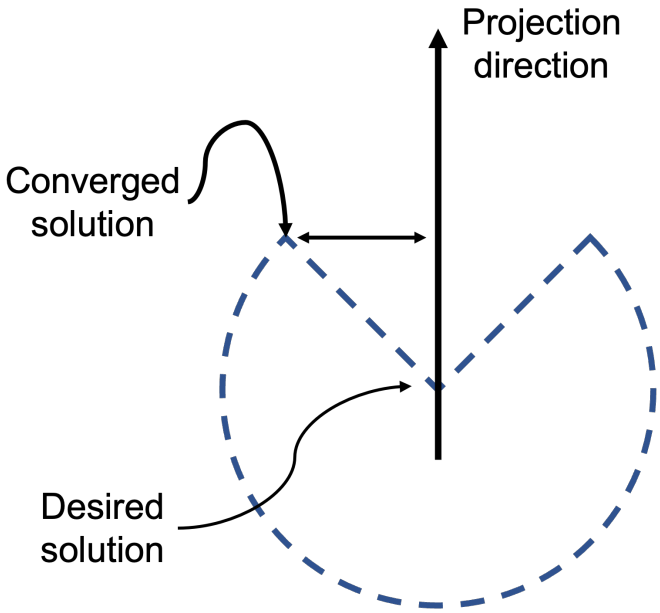

Fig. 1 In this stylized example, the converged solution point is further along the projection direction but not parallel to the projection direction. The desired solution and all points within the concave region may be missed.

Trade-offs were required to achieve speed and stability of these two algorithms which has implications for SSA applications. The use of a Gaussian level set to approximate the uncertainty in the initial states[1] allows for the algorithm to solve for the deviation in the initial states without requiring numerical iterations. However, this use introduces a potential limitation. If non-Gaussian errors are more important than speed or stability, the boundary conditions will have to be modified.

4 Numerical Examples

This section provides various examples to highlight the performance and utility of the algorithms. The algorithms were implemented in C++ on an M1 MacBook Pro from 2020, using the Boost Libraries for integration. In particular, a Fehlberg 78 order integrator with error tolerances $\leq 10^{-13}$. The Armadillo matrix library[13, 14] was used for matrix/vector support. The JPL SPICE libraries[15, 16] and DE440 ephemerides [17] are also used. Plotting was done

in spacekit.js[1]. Parallel processing leveraged the BOOST ASIO library. The reference frame was ECLIPJ2000, the specific impulse was set to 3,000 seconds, and the Sun, Earth, and Moon are included in the force model. The gravitational parameters used are $1.32712440018 \times 10^{11}$, 4.03503235×10^{5}, 4.902799×10^{3}, respectively. The units are km^3/s^2.

Five examples are provided to demonstrate the uses of the algorithm (see Table 1 for a summary). Case 1 is a reachability example on an elliptical orbit around Earth, with no significant multibody effects. The goal of case 1 is to show how the FFOE and OLE compare to one another. Case 2 is also a reachability case with a lunar flyby. Case 2 shows that the FFOE algorithm works well with strong multibody interactions. Case 3 runs case 2 backwards in time, highlighting how the algorithm can be used for controllability problems. Case 4 is a reachability case (the same as case 2) but with uncertain (Gaussian level set) initial conditions. Case 4 shows that the algorithm can be used for SSA algorithms. Case 5 is a controllability case (the same as case 3) but with uncertainty in terminal conditions. Case 5 highlights how the algorithm can be used to identify "watch corridors" if there is concern with objects attempting to rendezvous with other space objects.

Case	Multibody	Problem Type	Boundary Conditions	Algorithm Tested
1	No	Reachability	Fixed	FFOE and OLE
2	Yes	Reachability	Fixed	FFOE and OLE
3	Yes	Controllability	Fixed	FFOE
4	Yes	Reachability	Gaussian level set	FFOE
5	Yes	Controllability	Gaussian level set	FFOE

Table 1 Numerical cases cover a range of dynamics, problem types, and boundary conditions.

4.1 Case 1

The first case represents a near, two-body multirevolution (3.3 revolutions) reachability case. The initial orbit is an elliptical trajectory with no significant multibody effects. The simulation parameters are a max thrust of 0.01 N, 200 segments, and segment duration of 7,200 seconds.

The reachable set is computed using the first order methods and the open-loop method. Fig. (2) shows that both the FFOE solution and OLE solution produce similar results. The computational times are 0.27 seconds and 4.32 seconds for the FFOE and OLE solutions, respectively.

4.2 Case 2

The second case is a multibody reachability case. The trajectory has a close approach to the moon, resulting in strong multi-body effects and an inclination and energy increase. Although, the first order method produces a good

[1] https://typpo.github.io/spacekit/

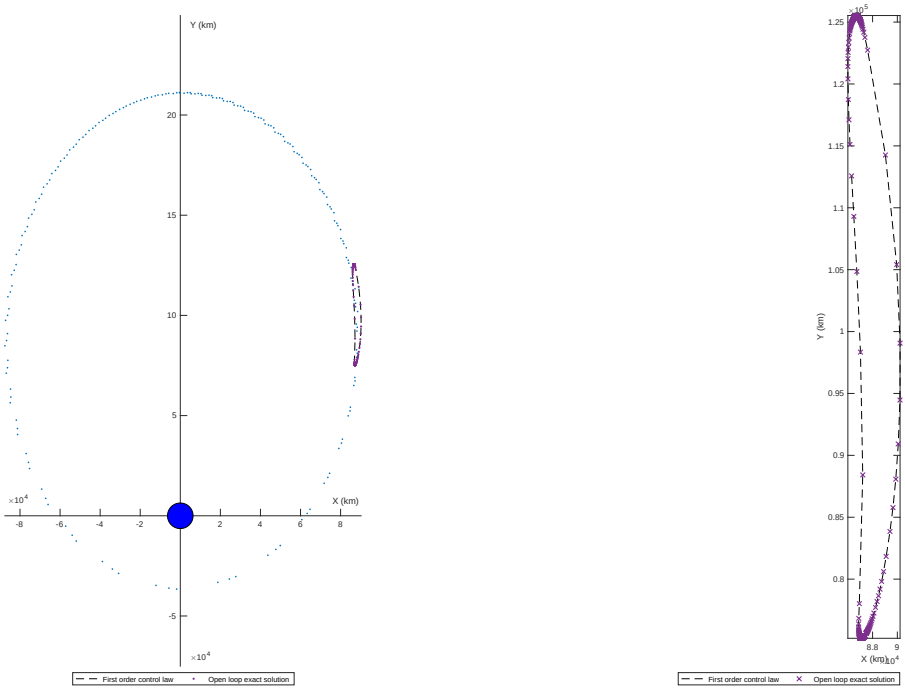

Fig. 2 Case 1 using an elliptical trajectory around Earth with no significant multi-body interaction. The epoch and initial conditions are 64.1 seconds and $x^0 = [0, 210820, 0, 0.753136347, 0, 0, 1000]$ Units are km, km/s, and kg. The FFOE and OLE algorithm produce similar results. Hints of he limitations of the OLE algorithm are noticeable as it produces bunching at the edges.

estimate of the reachable set, Fig. (3) shows that the exact method does a better job. Fig. (4) shows the entire trajectory projected onto the X-Y plane relative to the Earth and Moon.

The simulation parameters are a max thrust of 0.02 N, 200 segments, and segment duration of 7,200 seconds. The computation times of the FFOE and OLE algorithms are 0.25 seconds and 6.42 seconds, respectively. Fig. (5) and Fig. (6) highlight the three-dimensional nature of the trajectories by showing the close approach and inclination change.

4.3 Case 3

For the third case, a controllability case, the algorithms start at the end of case 2 and integrate the trajectory backwards. This case shows the range of initial conditions that would allow the spacecraft to still reach the terminal state. The simulation parameters are a max thrust of 0.02 N, 200 segments, and segment duration of -7,200 seconds. Fig. (7) shows the simulation results.The reference trajectory is the same as in case 2. For this controllability problem, the FFOE algorithm is able to identify the envelope of initial conditions that enable the final states in case 2 to be reached.

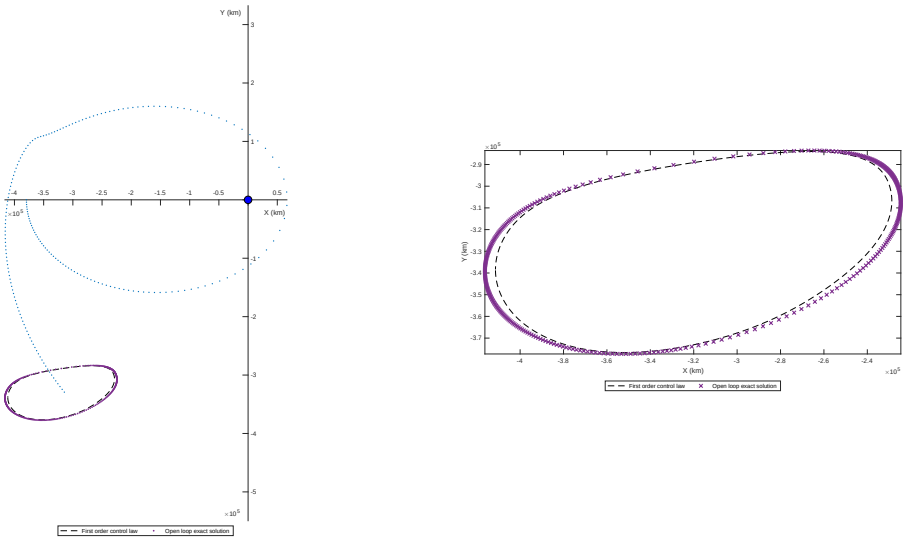

Fig. 3 Case 2 includes gravity of the Earth, Sun, and Moon and the spacecraft has a close flyby of moon. The FFOE and OLE algorithms show good agreement in their estimate of the reachable set. The OLE solution shows that the edges are the most underestimated by the FFOE algorithm. The epoch and initial conditions are 1072864.169 seconds and $x^0 = [-379476, 0, 0, 0, -0.561354689, 0, 1000]$. Units are km, km/s, and kg.

4.4 Case 4

The fourth case is the same as case 2 but with uncertain (Gaussian level set) initial conditions. The initial position is treated as uncertain but constrained to a 500 km unit sphere. The initial uncertainty envelope is visualized in Fig. (8), while the reachable set is shown in Fig. (9).

4.5 Case 5

The fifth case is is the same as case 3 (controllability example) but with uncertain initial conditions. The position is treated as uncertain and it lies on a 5,000 km unit sphere. The initial uncertainty envelope is visualized in Fig. (10). The XY view of the reachable set is shown in Fig. (11); Fig. (12) shows how with uncertainty the controllable set is contorted and expanded.

5 Conclusion

In this paper, a fast and automated algorithm for estimating EP spacecraft's reachable and controllable sets was derived and developed. Speed and automation are achieved through the novel use of an indirect multistage formulation. Speed is achieved because the algorithm only requires a single first order integration to estimate the control laws for the reachable set. The indirect multistage formulation also allows us to avoid solving a two-point boundary value problem thereby, allowing for a fully automated algorithm that requires only

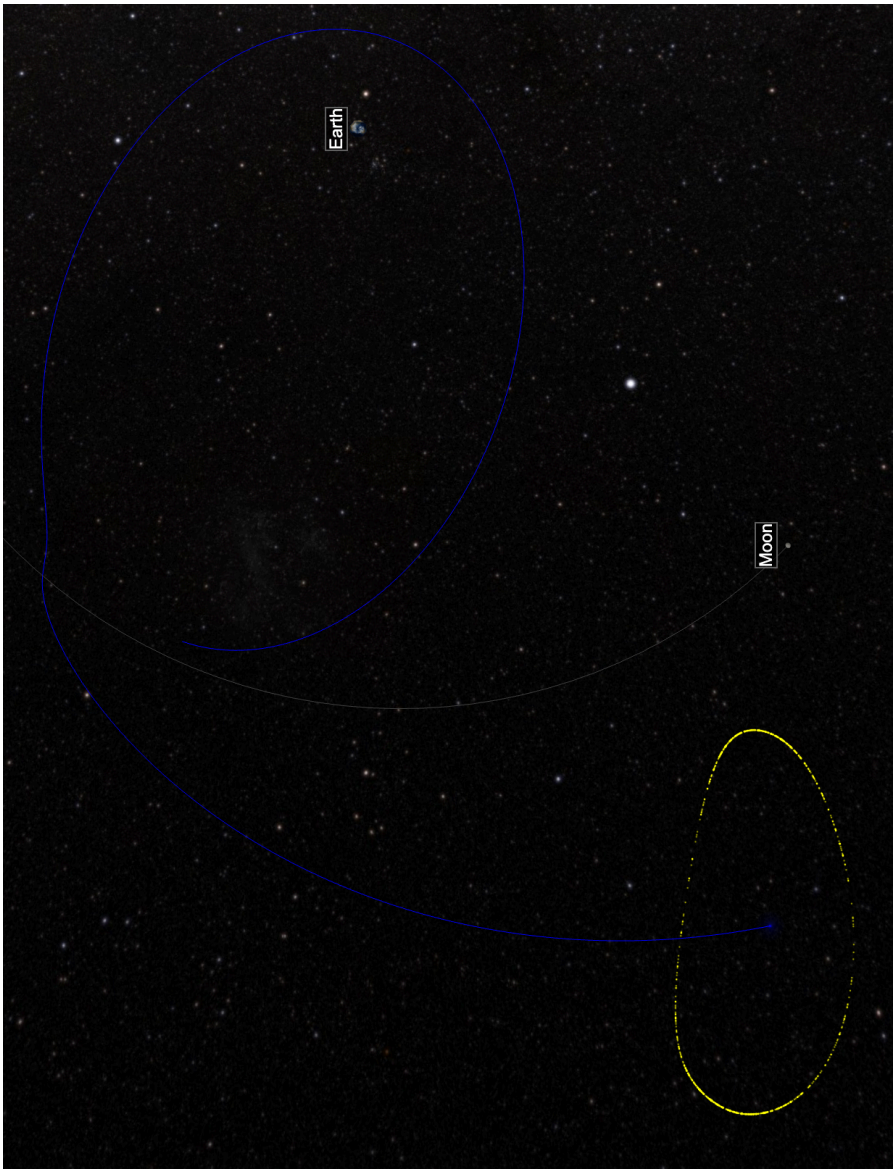

Fig. 4 The FFOE estimate for Case 2 (reachability) visualized with the final location of the Earth and moon shown.

knowing the spacecraft states. The algorithm can accommodate Gaussian level sets while retaining computational efficiency and automation. The Gaussian level set assumption can be useful for certain SSA applications. Additional boundary conditions can be used but may require trading away computational efficiency and algorithmic stability. Finally, the FFOE algorithm provides a good estimate of the reachable set and works well in multibody cases, such

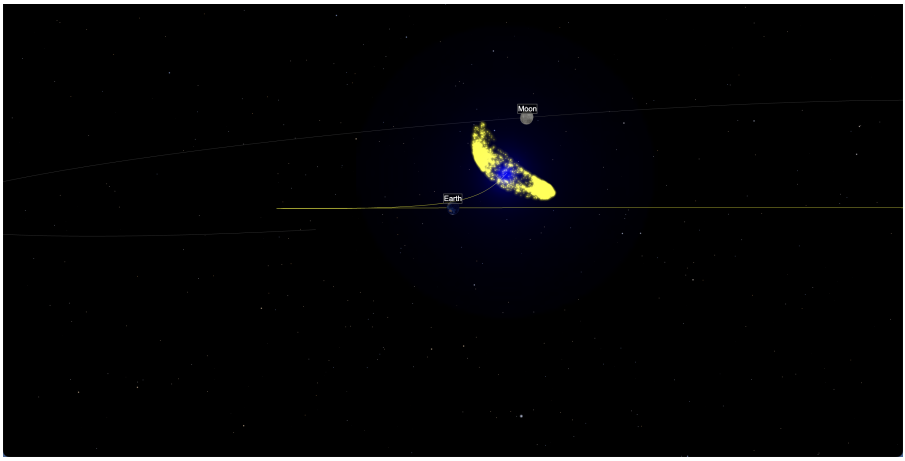

Fig. 5 Case 2 reachable set during a close approach of the moon

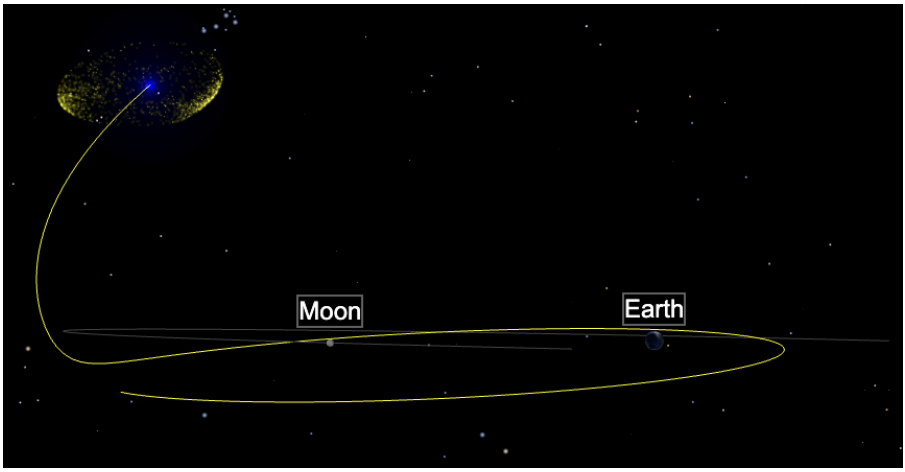

Fig. 6 A side view of case 2's trajectory and reachable set to highlight the plane change caused by the spacecraft's interaction with the moon.

as cislunar. Long timescales, high thrust, and interactions between the reachable set and gravitational centers can invalidate the results of both algorithms. The FFOE algorithm's speed and high level of automation means that it may provide value in large scale SSA applications or other applications such as trajectory design.

6 Acknowledgements

The authors thank Jim Thorne, Greg Davis, Stefania Brown-VanHoozer, and the anonymous reviewers for providing valuable suggestions that helped improve this work. We thank Dr. Lindsay Millard for raising the need for

additional research into reachability of electric propulsion spacecraft to our attention. We also thank Professor Taheri for replicating Case 1 and helping to identify that the numerical examples used the Earth-Moon gravitational parameter for Earth. The Institute for Defense Analyses (IDA) graciously provided funding to publish this research. On behalf of all authors, the corresponding author states that there is no conflict of interest.

References

[1] Holzinger, M.J., Scheeres, D.J.: Reachability results for nonlinear systems with ellipsoidal initial sets. IEEE transactions on aerospace and electronic systems **48**(2), 1583–1600 (2012)

[2] Holzinger, M.J., Scheeres, D.J., Erwin, R.S.: On-orbit operational range computation using gauss's variational equations with j 2 perturbations. Journal of Guidance, Control, and Dynamics **37**(2), 608–622 (2014)

[3] Aguilar Marsillach, D., Holzinger, M.J.: Spacecraft custody maintenance and maneuver detection using robotic telescopes and reachable sets. Journal of Guidance, Control, and Dynamics **44**(4), 667–683 (2021)

[4] Chilan, C.M., Conway, B.A.: A reachable set analysis method for generating near-optimal trajectories of constrained multiphase systems. Journal of Optimization Theory and Applications **167**(1), 161–194 (2015)

[5] Chen, Q., Qiao, D., Wen, C.: Minimum-fuel low-thrust trajectory optimization via reachability analysis and convex programming. Journal of Guidance, Control, and Dynamics **44**(5), 1036–1043 (2021)

[6] Rao, A.V.: A survey of numerical methods for optimal control. Advances in the Astronautical Sciences **135**(1), 497–528 (2009)

[7] Sims, J.A., Finlayson, P.A., Rinderle, E.A., Vavrina, M.A., Kowalkowski, T.D.: Implementation of a Low-Thrust Trajectory Optimization Algorithm for Preliminary Design. (2006)

[8] Bryson, A.E., Ho, Y.-C.: Applied Optimal Control: Optimization, Estimation, and Control. Routledge, New York (2018)

[9] Thorne, J.D., Hall, C.D.: Minimum-time continuous-thrust orbit transfers. The Journal of the astronautical sciences **45**(4), 411–432 (1997)

[10] Gurfil, P.: Modern Astrodynamics. Elsevier, Boston (2006)

[11] Bando, M., Scheeres, D.J.: Nonlinear attractive and reachable sets under optimal control in three-body problem. Journal of guidance, control, and dynamics **41**(8), 1766–1775 (2018)

[12] Patel, P., Scheeres, D.: No Initial Guess Required: Rapidly Computing the Feasible Set of Fuel-Optional Electric Propulsion Trajectories. (2023). AAS/AIAA

[13] Sanderson, C., Curtin, R.: Armadillo: a template-based c++ library for linear algebra. Journal of Open Source Software **1**(2), 26 (2016)

[14] Sanderson, C., Curtin, R.: An adaptive solver for systems of linear equations. In: 2020 14th International Conference on Signal Processing and Communication Systems (ICSPCS), pp. 1–6 (2020). IEEE

[15] Acton Jr, C.H.: Ancillary data services of nasa's navigation and ancillary information facility. Planetary and Space Science **44**(1), 65–70 (1996)

[16] Acton, C., Bachman, N., Semenov, B., Wright, E.: A look towards the future in the handling of space science mission geometry. Planetary and Space Science **150**, 9–12 (2018)

[17] Park, R.S., Folkner, W.M., Williams, J.G., Boggs, D.H.: The jpl planetary and lunar ephemerides de440 and de441. The Astronomical Journal **161**(3), 105 (2021)

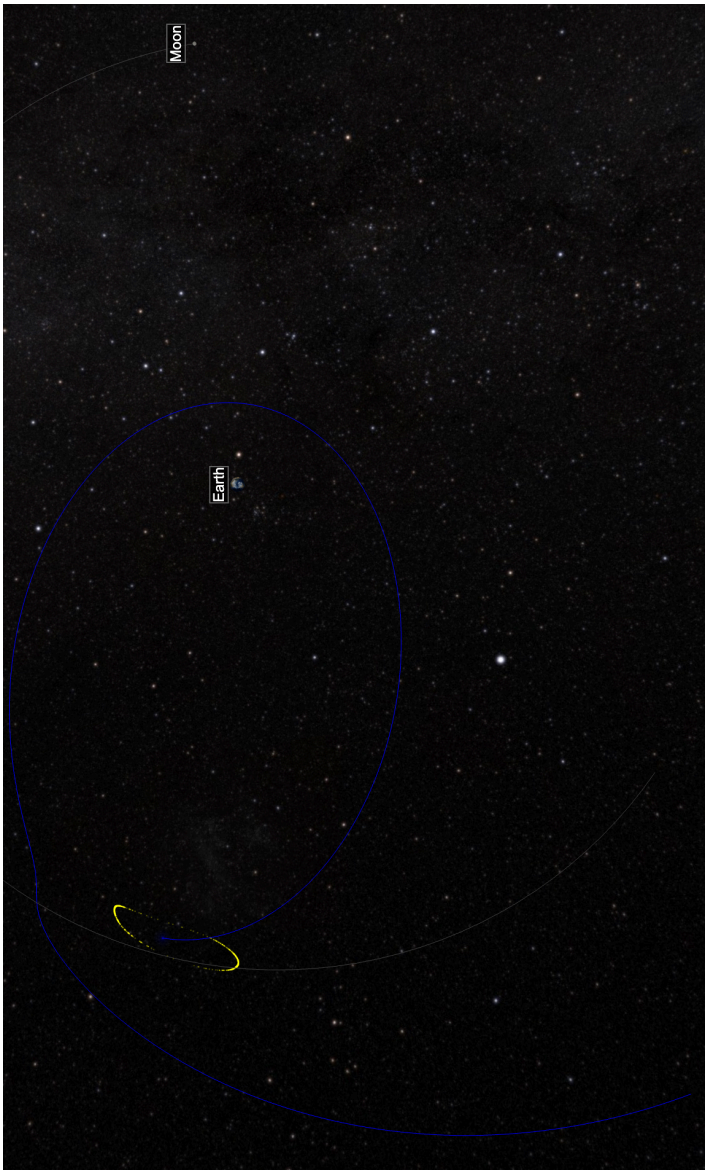

Fig. 7 Case 3 is case 2 run backwards in time. This represents a controllability case that shows the set of initial conditions that can achieve the terminal conditions in case 2. The epoch and initial conditions are 2512864.169 seconds and $x^0 = [-314562.64, -329219.31, 237676.53, 0.5262560, -0.65552567495712999, 0.1763679, 1000.0]$. Units are km, km/s, and kg.

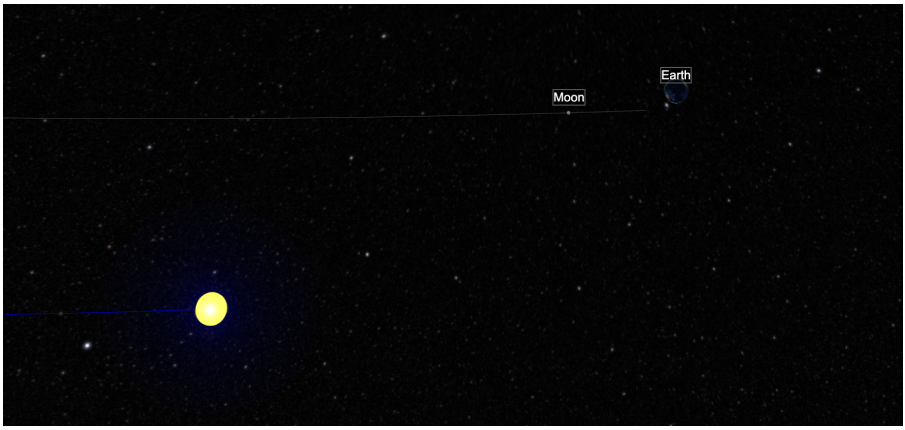

Fig. 8 The initial position uncertainty associated with case 4. Case 4 is a reachable set using the same conditions as case 2 with the addition of Gaussian level set uncertainty in the initial position.

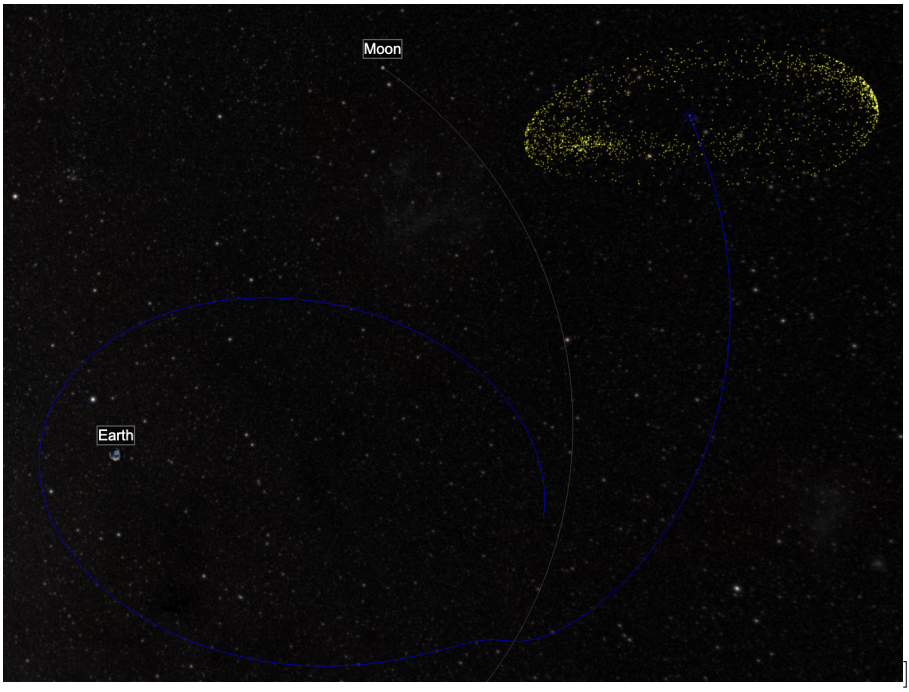

Fig. 9 The reachable set for case 4. The reachable set is more dispersed than case 2 because case 4 allowed for uncertainty in the initial position.

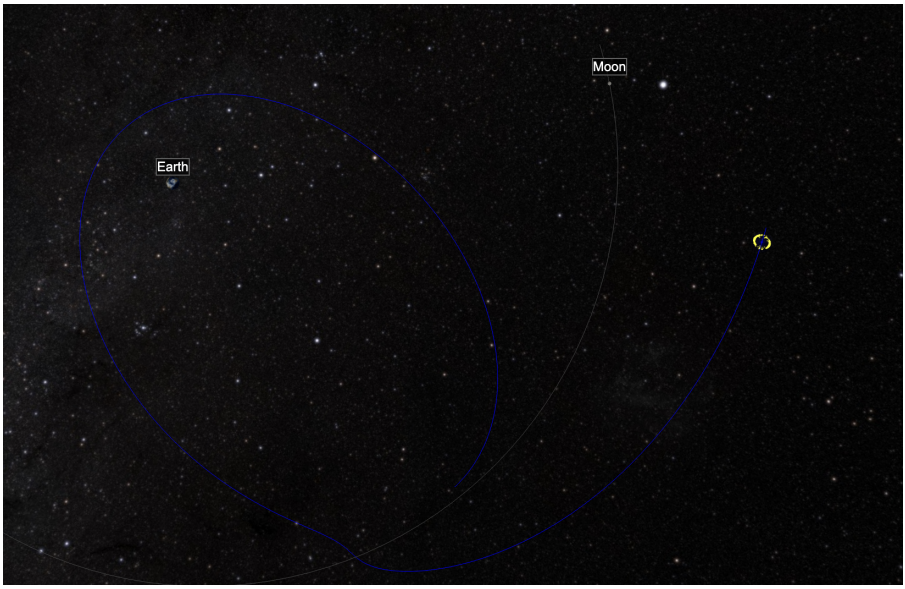

Fig. 10 The initial position uncertainty range for case 5, a controllability example, using the same inputs as case 3 with initial uncertainty.

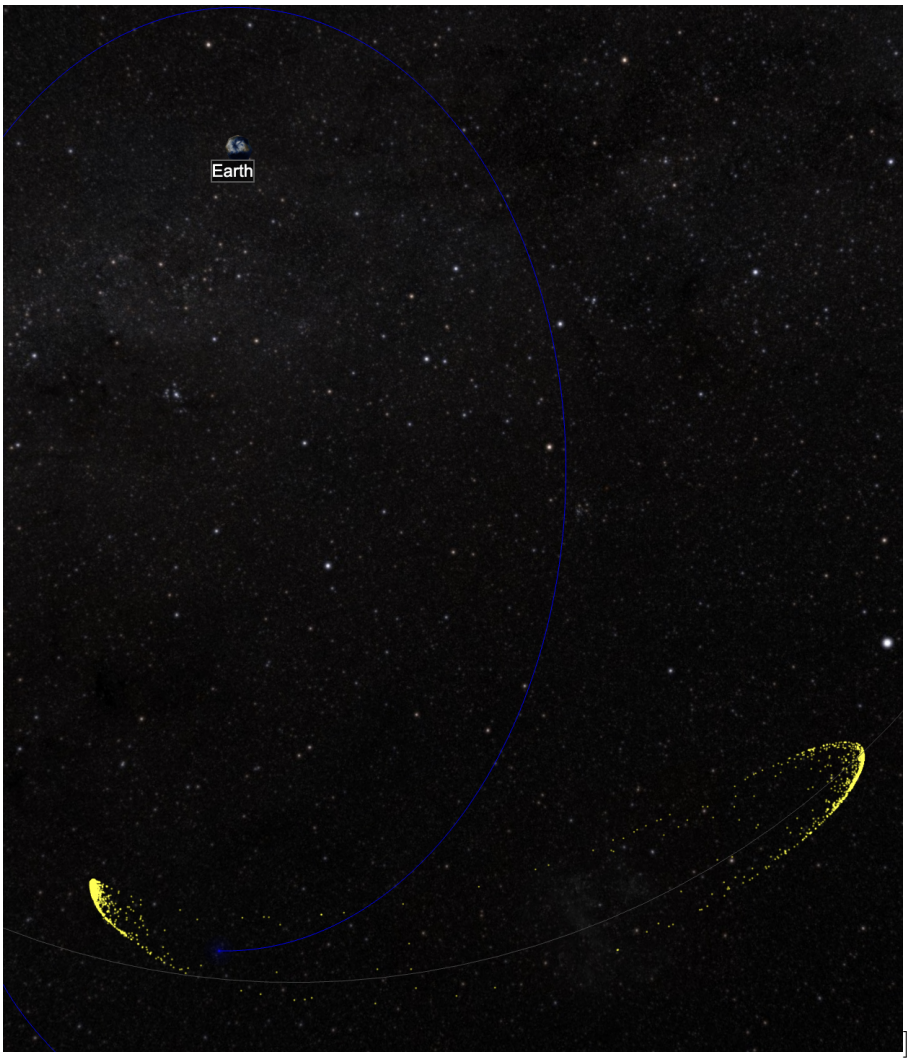

Fig. 11 The controllable set for case 5 is larger than case 3 because of the initial uncertainty in the spacecraft's position.

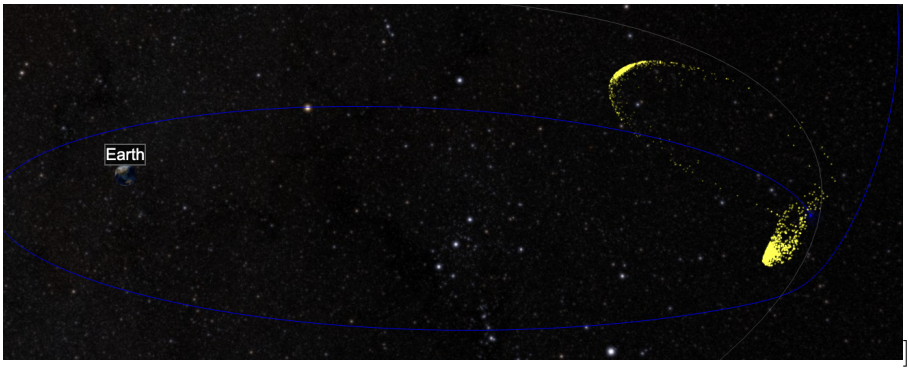

Fig. 12 A skewed view of case 5's to show the contorted nature of the controllable set.

REPORT DOCUMENTATION PAGE

PLEASE DO NOT RETURN YOUR FORM TO THE ABOVE ORGANIZATION

1. REPORT DATE	2. REPORT TYPE	3. DATES COVERED	
		START DATE	END DATE
xx-09-2023	Final	Dec 2022	Jan 2023

4. TITLE AND SUBTITLE

Rapid and Automatic Reachability Estimation of Electric Propulsion Spacecraft (Journal Article)

5a. CONTRACT NUMBER	5b. GRANT NUMBER	5c. PROGRAM ELEMENT NUMBER
HQ0034-19-D-0001		
5d. PROJECT NUMBER	**5e. TASK NUMBER**	**5f. WORK UNIT NUMBER**
C7265		

6. AUTHOR(S)

Patel, Prashant, R.
Scheeres, Daniel, J.

7. PERFORMING ORGANIZATION NAME(S) AND ADDRESS(ES)	8. PERFORMING ORGANIZATION REPORT NUMBER
Institute for Defense Analyses / Systems and Analyses Center Research Division 730 East Glebe Road Alexandria, Virginia 22305	IDA Document NS D-33192 Log #: H 23-000008

9. SPONSORING/MONITORING AGENCY NAME(S) AND ADDRESS(ES)	10. SPONSOR/MONITOR'S ACRONYM(S)	11. SPONSOR/MONITOR'S REPORT NUMBER
Institute for Defense Analyses / Systems and Analyses Center Research Division 730 East Glebe Road Alexandria, Virginia 22305	IDA / SAC	

12. DISTRIBUTION/AVAILABILITY STATEMENT

Distribution Statement A. Approved for public release; distribution is unlimited.

13. SUPPLEMENTARY NOTES

14. ABSTRACT

Reachable and controllable sets for electric propulsion spacecraft are important to many problems including: dynamic replanning, robust mission design, space situational awareness, assessing advanced concepts, and threat assessments. Current methods result in a twopoint boundary value problem or are limited in their application. The reachable and controllable problem is solved using an multistage indirect approach. The paper demonstrates our formulation enables rapid, reliable, and autonomous estimates of the reachable and controllable sets. Numerical examples show that the algorithms work in strong multibody environments (i.e., flybys) and incorporates uncertainty in initial conditions. These conditions make the algorithm suitable for space situational awareness and cislunar applications.

15. SUBJECT TERMS

Reachability; electric propulsion; automated; space situational; awareness

16. SECURITY CLASSIFICATION OF:			17. LIMITATION OF ABSTRACT	18. NUMBER OF PAGES
a. REPORT	b. ABSTRACT	c. THIS PAGE		
U	U	U	UU	30

19a. NAME OF RESPONSIBLE PERSON	19b. PHONE NUMBER
Patel, Prashant, R.	(703) 575-1439